RESEARCH ARTICLE

ADVANCED OPTICAL MATERIALS
www.advopticalmat.de

Observation of Magnetic Quadrupole Endowed Helical Dichroism in Artificial Propeller Meta-Molecules

Chang-Yin Ji, Shibo Xu, Qinghua Liang, Xiaochen Zhang, Xiaorong Hong, Yang Wang, Xiaowei Li, Lan Jiang, Yeliang Wang, Jincheng Ni, Dong Wu,* and Jiafang Li**

This study demonstrates that the magnetic quadrupole (MQ) can make an indispensable contribution to helical dichroism (HD), which is distinct from HD caused by electric quadrupole (EQ). Specifically, the established multipole expansion theory of the light–matter interaction reveals that EQ-induced HD belongs to the pure electric dipole–quadrupole (E1-E2) excitation, while newly discovered MQ-induced HD belongs to the pure magnetic dipole-quadrupole (M1-M2) excitation. Metallic propeller meta-molecules are used to elaborate on this novel physical mechanism and demonstrate that HD can be significantly enhanced and flexibly tuned by increasing stereo twist of propeller meta-molecules or slightly focusing the linearly polarized vortex beam to improve the orbital angular momentum number. Importantly, the aforementioned intriguing phenomena are validated by fabricating stereo twisted propeller meta-molecules via nano-kirigami method. The findings reveal a paradigm-shift approach to manipulate the chiroptical response of a single metallic nanostructure via photonic orbital angular moment, opening prospects for optical encryption, communication, next-generation chiroptical spectroscopy, and chiral vortex optical devices.

C.-Y. Ji, Q. Liang, X. Zhang, X. Hong, Y. Wang, J. Li
Key Lab of Advanced Optoelectronic Quantum Architecture and Measurement (MOE)
Beijing Key Lab of Nanophotonics & Ultrafine Optoelectronic Systems, and School of Physics
Beijing Institute of Technology
Beijing 100081, China
E-mail: jiafangli@bit.edu.cn

C.-Y. Ji, Y. Wang
School of Integrated Circuits and Electronics
MIIT Key Laboratory for Low-Dimensional Quantum Structure and Devices
Beijing Institute of Technology
Beijing 100081, China

S. Xu, J. Ni, D. Wu
CAS Key Laboratory of Mechanical Behavior and Design of Materials
Department of Precision Machinery and Precision Instrumentation
University of Science and Technology of China
Hefei, Anhui 230027, China
E-mail: njc@ustc.edu.cn; dongwu@ustc.edu.cn

X. Li, L. Jiang
Laser Micro/Nano Fabrication Laboratory
School of Mechanical Engineering
Beijing Institute of Technology
Beijing 100081, China

The ORCID identification number(s) for the author(s) of this article can be found under https://doi.org/10.1002/adom.202302795

DOI: 10.1002/adom.202302795

1. Introduction

The chiral light-matter interaction is one of the most flourishing realms of modern optics as it involves and intersects many disciplines from physics to chemistry and biology.[1–7] The spin angular momentum (SAM) of light is widely adopted to explore advanced chiroptical physics.[8–11] However, circularly polarized light (CPL) interacts weakly with a single chiral nanostructure for the case where the operating wavelength and structure size do not match. Thus, finding new physical mechanisms to enhance weak chiral signals is an important direction that researchers have been working on. Light field with orbital angular momentum (OAM) is also known as vortex beam which has been well applied in optical tweezers,[12] communication,[13] manufacturing,[14] etc.[15,16] The helical wavefront also gives vortex beam a chiral degree of freedom and its handedness is determined by the sign of the OAM munber l.[17–19] Interestingly, recent theoretical and experimental studies have demonstrated that the interaction between vortex beam and chiral matters depends on the sign of l.[20–30] This suggests that photonic OAM can provide another promising approach to investigate chiral physics. The giant helical dichroism (HD) has been achieved for a single helix,[25,29] planar-chiral nanostructure,[26] twisted stereometamaterial,[27] and chiral oligomer.[28] With the virtues of HD spectroscopy, enantiomeric distinction can be performed using monochromatic linearly polarized light fields, which is completely different from circular dichroism spectroscopy methods.

Although substantial progress has been made in the study of HD, the physical mechanism of chiroptical effect caused by photonic OAM is still elusive, especially for artificial chiral micro/nanostructures. The chiral light-matter interaction can be understood within the framework of multipole form refs. [31, 32]. Previous studies have shown that linearly polarized paraxial vortex beams cannot engage with chiral matters under the dipole moment approximation.[33–35] However, a chiral dipolar scatterer can produce HD when the vortex beam is tightly focused to produce the conversion of OAM to SAM.[23] In the paraxial regime, it is shown that the contribution of the electric quadrupole (EQ) plays a fundamental role in the chiral interaction between molecules and photonic OAM,[33,36] as shown

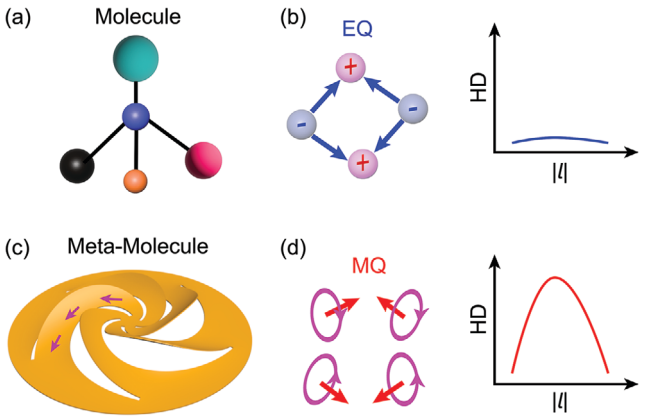

Figure 1. Helical dichroism (HD) mechanism. a) Schematic plot of chiral molecules. b) Electric quadrupole (EQ) and EQ-induced HD for chiral molecules in (a). HD is very small due to weak EQ excitation of chiral molecules. c) Schematic plot of artificial propeller meta-molecules. d) Magnetic quadrupole (MQ) and MQ-induced HD for the chiral meta-molecules in (c). Strong excitation of MQ significantly enhances HD. The magenta arrow in (c) indicates the current direction on certain blade.

in **Figure** 1a, b. This physical mechanism has been confirmed in molecular systems with nanoparticle aggregates[20] and nonlinear absorption.[30] HD is usually small due to weak chiral EQ excitation in molecular systems [see Figure 1b]. Until now, the EQ generated HD is only verified in a system with its size much smaller than the operating wavelength[20,30] but has not been verified in large-size chiral scatterer systems.[25–29] In addition, it is unclear whether there are other new physical mechanisms that produce HD.

Here, we reveal a conceptually new form of HD mechanism based on the magnetic quadrupole (MQ) excitation, as shown in Figure 1c, d. We first use multipole expansion theory to model this novel physical mechanism. We then theoretically engineer propeller meta-molecules [see Figure 1c] to explore MQ enabled HD, revealing that HD can be significantly enhanced and flexibly tuned by stereo twist of propeller meta-molecules or slightly focused vortex beam. Finally, we use the nano-kirigami method to prepare high-quality propeller meat-moleculars and experimentally observe the theoretically predicted phenomena. Our work advances the understanding of photonic OAM interactions with chiral matter and may provoke exciting frontiers for next-generation chiroptical spectroscopy and chiral vortex optical devices.

2. Results

The rate of excitation Γ for light-matter interaction is given by the time-averaged multipole form refs. [37–39],

$$\Gamma = \langle \dot{\boldsymbol{p}} \cdot \boldsymbol{E} + \dot{\boldsymbol{m}} \cdot \boldsymbol{B} + \frac{1}{3}\dot{\boldsymbol{Q}}^{e} : \nabla \boldsymbol{E} + \frac{1}{3}\dot{\boldsymbol{Q}}^{m} : \nabla \boldsymbol{B} \rangle_{t} \tag{1}$$

where $\boldsymbol{p}$, $\boldsymbol{m}$, $\boldsymbol{Q}^{e}$, and $\boldsymbol{Q}^{m}$ are the induced electric dipole (ED), magnetic dipole (MD), EQ, and MQ moments, respectively. $\boldsymbol{\Theta} = \frac{1}{2}(\tilde{\boldsymbol{\Theta}} e^{-i\omega t} + \tilde{\boldsymbol{\Theta}}^{*} e^{i\omega t})$ represents a certain real physical quantity in Equation (1). The expansion form of the multipole is described as,

$$\begin{aligned}
\tilde{p}_{\alpha} &= \sum_{\beta} \tilde{p}_{\alpha\beta}\tilde{E}_{\beta} + \sum_{\beta} \tilde{G}_{\alpha\beta}\tilde{B}_{\beta} + \frac{1}{3}\sum_{\beta\gamma} \tilde{A}_{\alpha\beta\gamma}\nabla_{\beta}\tilde{E}_{\gamma} \\
\tilde{m}_{\alpha} &= \sum_{\beta} \tilde{m}_{\alpha\beta}\tilde{B}_{\beta} - \sum_{\beta} \tilde{G}_{\alpha\beta}\tilde{E}_{\beta} + \frac{1}{3}\sum_{\beta\gamma} \tilde{K}_{\alpha\beta\gamma}\nabla_{\beta}\tilde{B}_{\gamma} \\
\tilde{Q}^{e}_{\alpha\beta} &= \sum_{\gamma} \tilde{A}_{\gamma\alpha\beta}\tilde{E}_{\gamma} \\
\tilde{Q}^{m}_{\alpha\beta} &= \sum_{\gamma} \tilde{K}_{\gamma\alpha\beta}\tilde{B}_{\gamma}
\end{aligned} \tag{2}$$

$\tilde{p}_{\alpha\beta}$, $\tilde{m}_{\alpha\beta}$, and $\tilde{G}_{\alpha\beta}$ are the electric, magnetic and electric-magnetic dipole polarizability, respectively. $\tilde{A}_{\alpha\beta\gamma}$ and $\tilde{K}_{\alpha\beta\gamma}$ are the electric and magnetic dipole-quadrupole polarizability, respectively. We can find that some terms of Γ are closely related to the chiroptical response due to they change sign under spatial inversion operation,

$$\begin{aligned}
\Gamma_{E1-M1} &= \frac{\omega}{2} Im \sum_{\alpha\beta} \tilde{G}_{\alpha\beta}[B_{\beta}E^{*}_{\alpha} - E_{\beta}B^{*}_{\alpha}] \\
\Gamma_{E1-E2} &= \frac{\omega}{6} Im \sum_{\alpha\beta\gamma} \tilde{A}_{\alpha\beta\gamma}[E^{*}_{\alpha}\nabla_{\beta}\tilde{E}_{\gamma} + E_{\alpha}\nabla_{\beta}\tilde{E}^{*}_{\gamma}] \\
\Gamma_{M1-M2} &= \frac{\omega}{6} Im \sum_{\alpha\beta\gamma} \tilde{K}_{\alpha\beta\gamma}[B^{*}_{\alpha}\nabla_{\beta}\tilde{B}_{\gamma} + B_{\alpha}\nabla_{\beta}\tilde{B}^{*}_{\gamma}]
\end{aligned} \tag{3}$$

Γ_{E1-M1}, Γ_{E1-E2}, and Γ_{M1-M2} represent the electric–magnetic dipole (E1-M1), electric dipole –quadrupole (E1-E2) and magnetic dipole–quadrupole (M1-M2) coupling terms, respectively. It an be seen that the Γ_{E1-M1} does not contain linear l-dependent terms. Therefore, photonic OAM cannot produce chiral interactions with chiral substances under dipole approximation. The gradient of the electric field $\boldsymbol{E}$ in Γ_{E1-E2} gives the linear l-dependent term. This shows that the combinations of ED and EQ can give the HD, which has been confirmed by experimental results. Here, we reveal another novel mechanism by which the combination of MD and MQ can also generate HD, named Γ_{M1-M2}. The linear l-dependent terms in Γ_{M1-M2} come from the gradient of the magnetic field $\boldsymbol{B}$. Importantly, the Γ_{M1-M2} enabled HD belongs to purely magnetic effect, which is different from purely electric effect of Γ_{E1-E2}. It should be noticed that the modeled Γ_{M1-M2} term predicts that HD could be enhanced by higher values of $|l|$.

We engineer propeller meat-molecules to study proposed physical mechanisms, as shown in **Figure** 2a–c. Compared to propeller chirality in molecules,[40–43] the artificial propeller meta-molecules can be flexibly designed and their blades are defined by etched curves $\rho(\theta)$ of air slits.[10,44–46] Here, an equiangular spiral with fractal characteristics is used to design the blade with $\rho(\theta) = ae^{b\theta}$. The 2D [Figure 2a] to 3D [Figure 2b, c] transformation of propeller meta-molecular can be obtained by using the bilayer stress model established earlier.[47] H is the maximum deformation height.

To avoid photonic SAM caused chirality effects and oblique incidence enabled extrinsic chirality, linearly polarized vortex beam is perpendicularly incident on the propeller meta-molecules in

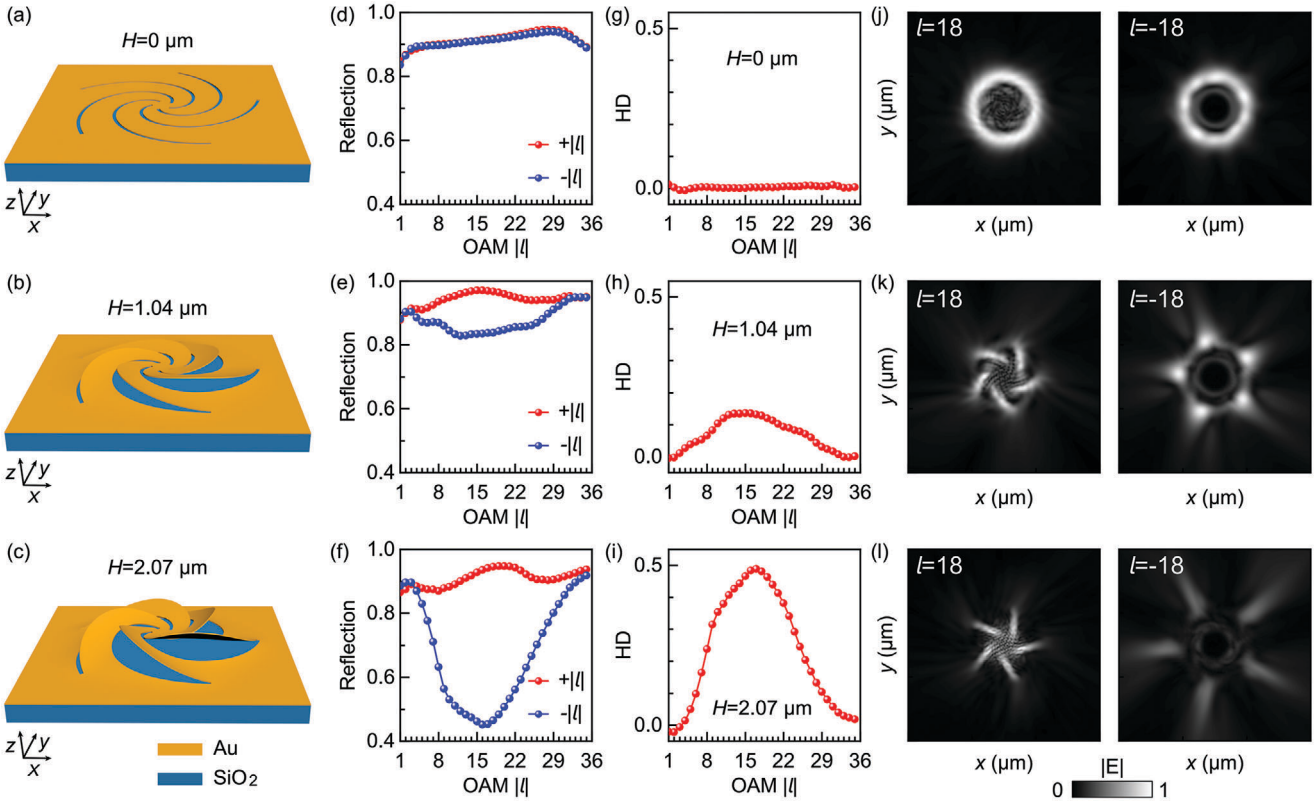

Figure 2. Stereo twist enhanced helical dichroism. a) The predesigned 2D propeller precursor with fivefold rotational symmetry. The substrate is silica. The air slit width and gold film thickness are 200 and 60 nm, respectively. The curve form of the etching air slit in polar coordinates is $\rho(\theta) = ae^{b\theta}$. Here, $a = 0.8$ μm, $b = 0.5$ and the range of parameter θ is $\theta \in [0, 4]$. b, c) The 3D stereo twisted propeller meta-molecules transformed from the 2D precursor in (a). H is the maximum deformation height. d–f) Reflection spectra of linearly polarized vortex beams corresponding to the propeller meta-molecules in (a-c). g–i) Helical dichroism (HD) spectra for the propeller meta-molecules in (a-c). j–l) The electric field distributions for the $l = \pm 18$. The ranges of x and y are both from -17.5 to 17.5 μm in (j–l).

Figure 2a–c. The beam waist radius w_0 of the vortex beam is $w_0 = 1.2$ μm for the results in Figure 2d–l. For $H = 0$ μm of the 2D propeller meta-molecular in Figure 2a, the results in Figure 2d shows that the reflectance spectra of opposite l is almost the same. However, when H increases to 1.04 μm, the reflection of $+|l|$ vortex beam is noticeably larger than that of the $-|l|$ vortex beam, as shown in Figure 2e. This shows that the chiroptical response caused by the photonic OAM comes from the 3D structural chirality. Interestingly, when the deformation height of the meat-molecular is further increased to 2.07 μm, the positive $+|l|$ vortex beam is still strongly reflected, while the reflection of the $-|l|$ vortex beam is greatly reduced, as shown in Figure 2f. In such case, the reflection differences in photonic OAM of opposite signs are significantly amplified for propeller meta-molecular in Figure 2c.

To quantify stereo twist-enhanced HD, the HD is defined as: $\mathrm{HD} = R_{+|l|} - R_{-|l|}$, where R is the reflectivity of vortex beam by chiral matters. For the 2D planar chiral meta-molecule in Figure 2a, the HD response is negligible [see Figure 2g] and such characteristic can also be revealed by the almost identical reflection field distribution in Figure 2j for $l = \pm 18$. Optically behaves like a mirror for the 2D structure in Figure 2a, see Figure 2j. As the blades twist height increases for the meta-molecules in Figure 2b, the distinct HD peak appears and the maximum HD value is 0.126, as shown in Figure 2h. Compared with the case of small twist height in Figure 2b, the results in Figure 2i show that the HD peak is more significant and the maximum HD value is 0.489 for large twist height in Figure 2c. The physical origin of giant HD peak can also be observed from remarkably incoordinate reflection field distribution between vortex beam with $l = 18$ and $l = -18$, as shown in Figure 2k, l. For 3D chiral structures in Figure 2b, c, the field distribution of the reflected vortex beam is significantly modulated and the strong reflection comes from the stereotwisted blades [see Figure 2k, l].

We use the multipole theory to further reveal that the strong HD comes from the chiral MQ excitation. **Figure** 3a,b is the scattering power spectra of multipole moments for the propeller meta-molecules in Figure 2b,c, respectively. Their common feature is the excitation amplitude of MQ is much greater than that of ED, MD, and EQ, as shown in Figure 3. Furthermore, the amplitude of the MQ excited by $+|l|$ vortex beam is greater than that of excited by $-|l|$ vortex beam for the same propeller meta-molecular, as shown in Figure 3c, d. This suggests that the HD indeed comes from the contribution of chiral MQ. Comparing the results in Figure 3c,d, it can be seen that the difference in magnitude of the MQ excited by the $+|l|$ and $-|l|$ vortex beams becomes larger as the twist height of the propeller meta-molecular increases. Such observation explains why deformation enhances HD and is self-consistent with the results in Figure 2. The strong

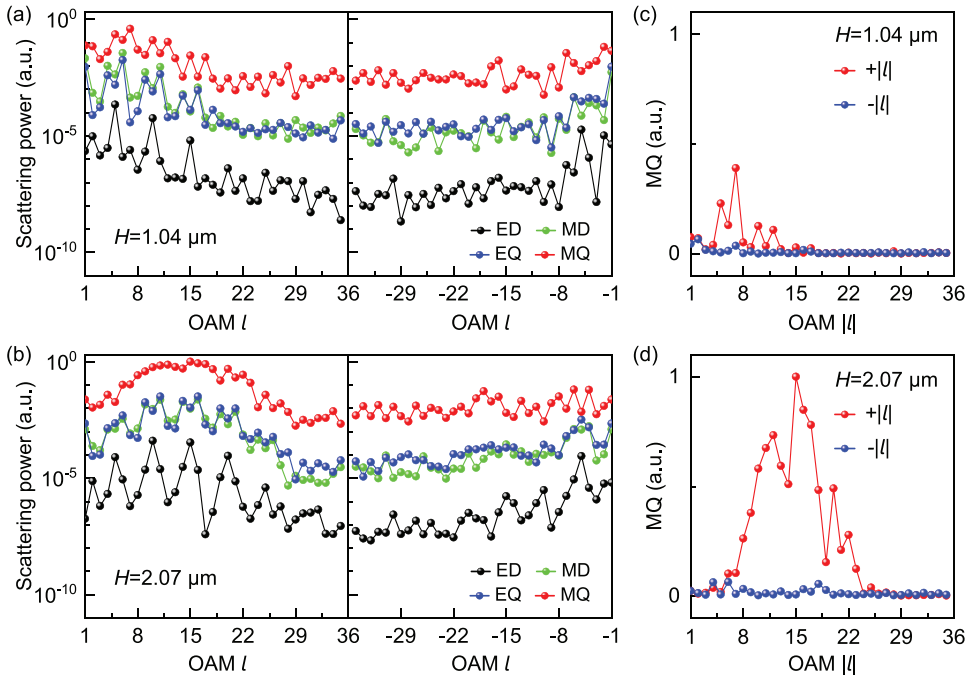

Figure 3. a, b) Scattering power spectra of multipole moments under linearly polarized vortex beam for the propeller meta-molecules in Figure 2b, c. c, d) Scattering power of MQ excited by the $+|l|$ and $-|l|$ vortex beams. ED: electric dipole; MD: magnetic dipole; EQ: electric quadruple; MQ: magnetic quadrupole. Scattering power normalized to the largest MQ.

excitation of the MQ benefits from the unique topological morphology of the propeller meta-moleculars, which are formed by the combination of five unidirectionally twisted blades. Electric current flows along the blades since the electron motion is confined to the interface between metal blades and air background, indicated by the magenta arrows in Figure 1c. This results in a configuration of the current on the propeller meta-molecule that resembles that of MQ.

Another property for MQ-induced HD is that HD can be enhanced by large OAM l due to Γ_{M1-M2} linear dependence on l. Here, we illustrate this phenomenon by changing the beam waist radius w_0, since the intensity of the vortex beam is a ring distribution of the central dark spot and the diameter of the ring profile is $d_l = w_0\sqrt{2|l|}$. The w_0 corresponding to **Figure 4a,b,c** is $w_0 =$ 2 μm, $w_0 = 1.5$ μm, and $w_0 = 1$ μm, respectively. From the results in Figure 4, it can be seen that as w_0 decreases, the position where the reflection difference between $+|l|$ and $-|l|$ vortex beam is large moves toward a large $+|l|$ value and the spectrum difference gradually increases. The corresponding HD spectra are shown in the bottom of Figure 4a–c. The $|l|$ corresponding to maximum HD value are $|l| = 6$ in Figure 4a, $|l| = 10$ in Figure 4b and $|l| = 17$ in Figure 4c. The maximum HD increases from 0.187 to 0.588 as l changes from 6 to 17, see Figure 4a, c.

The propeller meta-molecule designed in Figure 2 is experimentally fabricated through a cutting-edge nano-kirigami method.[47–49] **Figure 5a** is the scanning electron microscopy (SEM) image of the fabricated metallic propeller meta-molecules, which is consistent with the theoretical design structure in Figure 2c. It should be noticed that the slight collapse of the propeller precursor before the irradiation of FIB has little effect

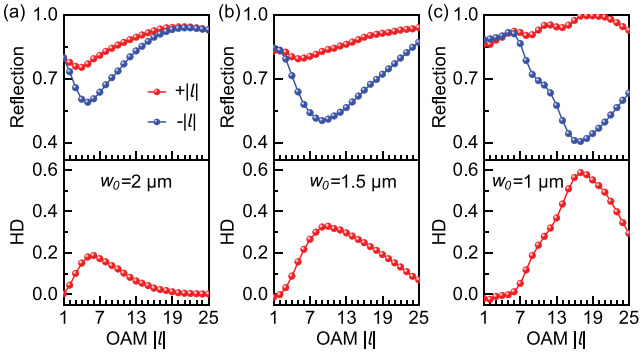

Figure 4. a–c) Reflection and HD spectra of linearly polarized vortex beams with different beam waist radius w_0 for the propeller meta-molecule in Figure 2c. $w_0 = 2\epsilon$m in (a), $w_0 = 1.5\epsilon$m in (b) and $w_0 = 1\epsilon$m in (c).

on the deformation during subsequent FIB irradiation since the slightly collapsed parts will be eventually deformed upward. In the experiment, FIB is used to irradiate the propeller structure from center to outside to achieve uniform structural deformation. The structural damage under FIB irradiation depends on factors such as ion species, energy, dose, and the nature of the material being irradiated. Here, when deforming a 2D precursor into a 3D propeller structure, we use very low dosage of FIB to avoid influential structural damage at the operation wavelength region (see sample fabrications of Experimental Section). Smooth surfaces reveal high-quality properties of chiral metallic nanostructures based on nano-kirigami method and negligible structural damage, which is difficult to obtain with

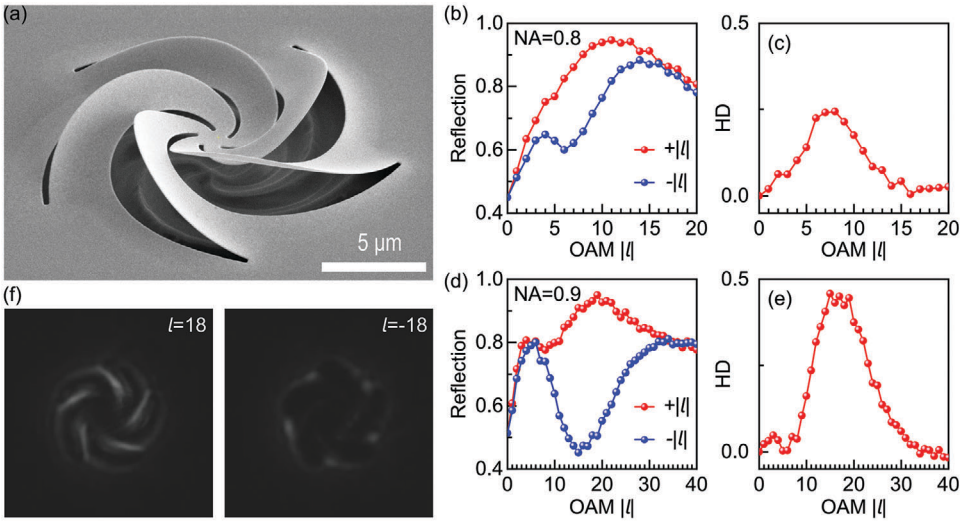

Figure 5. Experimental Observations. a) SEM image of the fabricated propeller meta-molecule. b–e) Measured reflection (b, d) and helical dichroism (c, e) spectra of the propeller meta-molecule in (a) with different NA. f) The light intensity distribution recorded by charge-coupled device (CCD) camera for NA=0.9. NA is the numerical aperture of microscope objective (MO). The linearly polarized vortex beam is focused by the MO and then illuminated vertically onto the sample. Scale bars: 5 μm.

other additive manufacturing technologies.[50–53] Experimental vortex beams with different OAM l are obtained by controlling fork grating holograms on a phase-only spatial light modulator. The linearly polarized vortex beam is slightly focused by the microscope objective (MO) and then incident on the sample vertically. The vortex beam with different beam waist radius is obtained by MO with different numerical aperture (NA).

The measured reflection and HD spectra are shown in Figure 5b–e, respectively. The NAs of the experimental results in Figure 5b–e are NA = 0.8 and NA = 0.9, respectively. The measured reflectance spectra are in good agreement with the theoretical simulation except for the small OAM case, unambiguously revealing that MQ-induced HD is successfully realized. The discrepancy between theory and experiment mainly comes from the difficulty in producing ideal vortex beam experimentally and the uncertainty of optical characterizations. The HD peak appears at the $|l| = 8$ and its intensity is 0.243 for NA = 0.8 [see Figure 5c], while HD peak appears at the $|l| = 17$ and its intensity is 0.45 for NA = 0.9 [see Figure 5e]. The experimental results show that HD can indeed be greatly enhanced by improving OAM l, which also provides solid evidence for the discovery of MQ-induced HD. Figure 5f is the reflection field distribution of $l = 18$ and $l = -18$ recorded by the charge-coupled device (CCD) camera for NA = 0.9. It can be clearly seen that the vortex beam with $l = 18$ is strongly scattered by the twisted blades, while the vortex beam of $l = -18$ interacts with the blades very weakly, resulting in a small reflection. It should be noticed that in the current reflection configurations, numerical simulations reveal that the shape or depth of the etched silica substrate basically does not affect the spectra (results not shown). Compared with the traditional helical structures, here the propeller structures could provide a higher degree of tunability in terms of twisted dimension, pitch angle, and geometric configuration, resulting in an efficient interaction with the incident vortex beam and enhanced HD response.

3. Conclusion

In summary, we theoretically propose and experimentally verify that the photonic orbital angular momentum can produce chiral interactions with the magnetic quadrupole excitation of chiral matters, which highlights the importance of often overlooked higher order multipole for the cases where the chiral light interacts with large-scale objects. We use the established multipole expansion theory to profoundly reveal that the magnetic quadrupole induced helical dichroism belongs to pure magnetic dipole-quadrupole coupling, which is different from the well-studied mechanism of electric quadrupole-induced helical dichroism. We design artificial propeller meat-moleculars based on nano-kirigami method to elaborate on this mechanism, showing that helical dichroism can be remarkably enhanced and flexibly manipulated by deformation of propeller meta-molecules or slightly focused vortex beam to improve the orbital angular momentum number. The found mechanism and unique propeller configuration could provide a new platform to investigate fascinating chiroptical physics and manipulate the photonic orbital angular momentum, paving the way for chiral vortex optical devices.

4. Experimental Section

Numerical Simulations: The mechanical transformations of the 2D precursors into the 3D propeller meta-molecules were implemented by adopting a bilayer stress distribution model with finite element method.[47] The optical reflectance spectra were simulated under linearly polarized vortex beam incidence that propagated along the −*z*-axis

direction based on a commercial finite difference time-domain-based software (Lumerical FDTD Solutions, Inc.). Perfectly matched layer boundaries were applied along the *x*-, *y*- and *z*-axis directions in the simulation. The electric field of incident linearly polarized vortex beams in the polar coordinate system is defined as follows,

$$E_l(r,\phi) = \frac{C}{\sqrt{|l|!}}\left(\frac{r}{w_0}\right)^{|l|} e^{-\frac{r^2}{w_0^2}} e^{il\phi}\hat{x} \quad (4)$$

where C, w_0, and l are the normalization constant, beam waist radius and orbital angular momentum number of the vortex beam, respectively. The incident wavelength is $\lambda = 0.8$ µm.

Sample Fabrications: The artificial propeller meta-molecules were fabricated by using the nano-kirigami method based on Au/SiO_2 substrate. The SiO_2 substrate allowed the 2D propeller precursor to maintain ideal flatness before transforming into a 3D propeller meta-molecule. The nano-kirigami method includes a two-dosage ion beam irradiation with focused ion beam (FIB) facility (Helios G4 UC). The 2D precursors were first cut by the FIB under high ion doses of 200 Cm^{-2} (30 kV, 40 pA). Then, the SiO_2 substrate under the 2D propeller precursor was etched with HF solution. Etch time was 25 min to fully suspend the 2D propeller precursor. The HF solution was made by diluting 40% hydrofluoric acid and water in a ratio of 1:4. After the wet-etching process, global ion beam irradiation was conducted by frame-scanning the effective sample area with a relatively low dose of 2–8 Cm^{-2}.

Optical Characterizations: A mode-locked Ti:sapphire ultrafast oscillator (Chameleon Vision-S, Coherent, Inc.), which had a central wavelength of 800 nm, a pulse width of 75 fs, and a repetition rate of 80 MHz, was used as the light source. A phase-only reflective liquid-crystal SLM (Pluto NIR-2, Holoeye Photonics AG) with 1920×1080 pixels was used to display computer-generated holograms in the experiment. A general dry objective lens (NA = 0.8/0.9, Olympus) was used to focus the generated vortex beams in the fabricated meta-molecules. The sample was mounted on a 3D-piezo-nanostage (E545, Physik Instrumente) with nanoscale resolution and a 200 µm × 200 µm × 200 µm traveling range to precisely tune the locations of nanostructures under optical microscopy. After positioning the single microstructure to the vortex beam axes, the reflected intensity was caught by a CCD (MindVision HD-SUA133GM-T camera, image area: 1280×1024 pixels) with the acquisition time of 30 ms. For a single chiral meta-molecule, all optical images were gathered within 5 min for calculating its reflection and HD spectra.

Acknowledgements

C.Y.J., S.X., and Q.L. contributed equally to this work. This work was supported by the National Natural Science Foundation of China (Grant nos. 12204041, 61975016, 92163206, 62375253, and 62325507), the Science and Technology Project of Guangdong (Grant no. 2020B010190001), China Postdoctoral Science Foundation (Grant no. 2021M700436), the National Key R&D Program of China (Grant no. 2021YFA1400100), Natural Science Foundation of Beijing Municipality (Grant nos. 1212013 and Z190006), and J.N. acknowledged the support from the start-up funding of University of Science and Technology of China and the CAS Pioneer Hundred Talents Program.

Conflict of Interest

The authors declare no conflict of interest.

Data Availability Statement

The data that support the findings of this study are available from the corresponding author upon reasonable request.

Keywords

chiral metallic nanostructures, helical dichroism, magnetic quadrupole, nano-kirigami, propeller meta-molecules, vortex beam

Received: November 5, 2023
Revised: December 11, 2023
Published online:

[1] V. K. Valev, J. J. Baumberg, C. Sibilia, T. Verbiest, *Adv. Mater.* **2013**, *25*, 2517.
[2] M. Hentschel, M. Schäferling, X. Duan, H. Giessen, N. Liu, *Sci. Adv.* **2017**, *3*, e1602735.
[3] E. S. Goerlitzer, A. S. Puri, J. J. Moses, L. V. Poulikakos, N. Vogel, *Adv. Opt. Mater.* **2021**, *9*, 2100378.
[4] L. A. Warning, A. R. Miandashti, L. A. McCarthy, Q. Zhang, C. F. Landes, S. Link, *ACS Nano* **2021**, *15*, 15538.
[5] C. Genet, *ACS Photonics* **2022**, *9*, 319.
[6] Y. Chen, W. Du, Q. Zhang, O. Ávalos-Ovando, J. Wu, Q.-H. Xu, N. Liu, H. Okamoto, A. O. Govorov, Q. Xiong, C.-W. Qiu, *Nat. Rev. Phys.* **2022**, *4*, 113.
[7] A. Lininger, G. Palermo, A. Guglielmelli, G. Nicoletta, M. Goel, M. Hinczewski, G. Strangi, *Adv. Mater.* **2023**, *35*, 2107325.
[8] J. K. Gansel, M. Thiel, M. S. Rill, M. Decker, K. Bade, V. Saile, G. von Freymann, S. Linden, M. Wegener, *Science* **2009**, *325*, 1513.
[9] Z. Liu, Y. Xu, C.-Y. Ji, S. Chen, X. Li, X. Zhang, Y. Yao, J. Li, *Adv. Mater.* **2020**, *32*, 1907077.
[10] C.-Y. Ji, S. Chen, Y. Han, X. Liu, J. Liu, J. Li, Y. Yao, *Nano Lett.* **2021**, *21*, 6828.
[11] B. Yao, Q. Wei, Y. Yang, W. Zhou, X. Jiang, H. Wang, M. Ma, D. Yu, Y. Yang, Z. Ning, *Nano Lett.* **2023**, *23*, 1938.
[12] M. Padgett, R. Bowman, *Nat. Photonics* **2011**, *5*, 343.
[13] A. E. Willner, K. Pang, H. Song, K. Zou, H. Zhou, *Appl. Phys. Rev.* **2021**, *8*, 4.
[14] J. Ni, C. Wang, C. Zhang, Y. Hu, L. Yang, Z. Lao, B. Xu, J. Li, D. Wu, J. Chu, *Light Sci. Appl.* **2017**, *6*, e17011.
[15] H. Ren, S. A. Maier, *Adv. Mater.* **2023**, *35*, 2106692.
[16] Y. Lu, Y. Xu, X. Ouyang, M. Xian, Y. Cao, K. Chen, X. Li, *Opto-Electron. Adv.* **2022**, *5*, 210014.
[17] J. Mun, M. Kim, Y. Yang, T. Badloe, J. Ni, Y. Chen, C.-W. Qiu, J. Rho, *Light Sci. Appl.* **2020**, *9*, 139.
[18] K. A. Forbes, D. L. Andrews, *J. Phys. Photonics* **2021**, *3*, 022007.
[19] D. L. Andrews, *Chirality* **2023**, *35*, 899.
[20] W. Brullot, M. K. Vanbel, T. Swusten, T. Verbiest, *Sci. Adv.* **2016**, *2*, e1501349.
[21] K. A. Forbes, D. L. Andrews, *Phys. Rev. A* **2019**, *99*, 023837.
[22] K. A. Forbes, D. L. Andrews, *Phys. Rev. Res.* **2019**, *1*, 033080.
[23] P. Woźniak, I. De Leon, K. Höflich, G. Leuchs, P. Banzer, *Optica* **2019**, *6*, 961.
[24] K. A. Forbes, G. A. Jones, *Phys. Rev. A* **2021**, *103*, 053515.
[25] J. Ni, S. Liu, D. Wu, Z. Lao, Z. Wang, K. Huang, S. Ji, J. Li, Z. Huang, Q. Xiong, Y. Hu, J. Chu, C.-W. Qiu, *Proc. Natl. Acad. Sci.* **2021**, *118*, e2020055118.
[26] J. Ni, S. Liu, G. Hu, Y. Hu, Z. Lao, J. Li, Q. Zhang, D. Wu, S. Dong, J. Chu, , C.-W. Qiu, *ACS Nano* **2021**, *15*, 2893.
[27] S. Liu, J. Ni, C. Zhang, X. Wang, Y. Cao, D. Wang, S. Ji, D. Pan, R. Li, H. Wu, C. Xin, J. Li, Y. Hu, G. Li, D. Wu, J. Chu, *Laser Photonics Rev.* **2022**, *16*, 2100518.
[28] Y. Cao, S. Liu, Y. Tao, X. Wang, J. Ni, C. Wang, X. Zheng, J. Li, Y. Hu, D. Wu, , J. Chu, *ACS Photonics* **2023**, *10*, 1873.
[29] N. Dai, S. Liu, Z. Ren, Y. Cao, J. Ni, D. Wang, L. Yang, Y. Hu, J. Li, J. Chu, D. Wu, *ACS Nano* **2023**, *17*, 1541.

[30] J.-L. Bégin, A. Jain, A. Parks, F. Hufnagel, P. Corkum, E. Karimi, T. Brabec, R. Bhardwaj, *Nat. Photonics* **2023**, *17*, 82.
[31] L. Barron, C. Gray, *J. Phys. A: Math., Nucl. Gen.* **1973**, *6*, 59.
[32] E. Graham, J. Pierrus, R. Raab, *J. Phys. B: At. Mol. Opt. Phys.* **1992**, *25*, 4673.
[33] M. Babiker, C. Bennett, D. Andrews, L. D. Romero, *Phys. Rev. Lett.* **2002**, *89*, 143601.
[34] D. Andrews, L. D. Romero, M. Babiker, *Opt. Commun.* **2004**, *237*, 133.
[35] F. Araoka, T. Verbiest, K. Clays, A. Persoons, *Phys. Rev. A* **2005**, *71*, 055401.
[36] K. A. Forbes, D. L. Andrews, *Optics Lett.* **2018**, *43*, 435.
[37] A. Buckingham, M. Dunn, *J. Chem. SOC. A: Inorg. Phys. Theor.* **1971**, *12*, 1988.
[38] N. Yang, A. E. Cohen, *J. Phys. Chem. B* **2011**, *115*, 5304.
[39] L. D. Barron, *Molecular light scattering and optical activity*, Cambridge University Press, Cambridge, **2009**.
[40] T. Kosaka, Y. Inoue, T. Mori, *J. Phys. Chem. Lett.* **2016**, *7*, 783.
[41] M. Toyoda, Y. Imai, T. Mori, *J. Phys. Chem. Lett.* **2017**, *8*, 42.
[42] Y. Zhang, J. P. Calupitan, T. Rojas, R. Tumbleson, G. Erbland, C. Kammerer, T. M. Ajayi, S. Wang, L. A. Curtiss, A. T. Ngo, S. E. Ulloa, G. Rapenne, S. W. Hla, *Nat. Commun.* **2019**, *10*, 3742.
[43] S. Liu, *J. Phys. Chem. Lett.* **2021**, *12*, 8720.
[44] X. Li, C.-Y. Ji, S. Chen, Y. Han, J. Liu, J. Li, *Adv. Opt. Mater.* **2021**, *9*, 2101191.
[45] S. Chen, C.-Y. Ji, Y. Han, X. Liu, Y. Wang, J. Liu, J. Li, *APL Photonics* **2022**, *7*, 5.
[46] S. Qiao, Q. Liang, X. Zhang, X. Liu, S. Feng, C.-Y. Ji, H. Guo, J. Li, *APL Photonics* **2022**, *7*, 11.
[47] Z. Liu, H. Du, J. Li, L. Lu, Z.-Y. Li, N. X. Fang, *Sci. Adv.* **2018**, *4*, eaat4436.
[48] J. Li, Z. Liu, *Nanophotonics* **2018**, *7*, 1637.
[49] Z. Liu, H. Du, Z.-Y. Li, N. X. Fang, J. Li, *APL Photonics* **2018**, *3*, 10.
[50] P. Galliker, J. Schneider, H. Eghlidi, S. Kress, V. Sandoghdar, D. Poulikakos, *Nat. Commun.* **2012**, *3*, 890.
[51] S. K. Seol, D. Kim, S. Lee, J. H. Kim, W. S. Chang, J. T. Kim, *Small* **2015**, *11*, 3896.
[52] C. W. Visser, R. Pohl, C. Sun, G.-W. Römer, B. Huis in 't Veld, D. Lohse, *Adv. Mater.* **2015**, *27*, 4087.
[53] L. Hirt, S. Ihle, Z. Pan, L. Dorwling-Carter, A. Reiser, J. M. Wheeler, R. Spolenak, J. Vörös, T. Zambelli, *Adv. Mater.* **2016**, *28*, 2311.